JOURNAL OF Materials CHEMISTRY

In-situ study of the solid–solid phase transitions occurring in real diesel wax crystalline systems using differential scanning calorimetry and high-resolution synchrotron X-ray powder diffraction

Steven R. Craig,[a]† Gerard P. Hastie,[b] Kevin J. Roberts,*[b] John N. Sherwood,[a] Robert D. Tack[c] and Robert J. Cernik[d]

[a]*Department of Pure and Applied Chemistry, University of Strathclyde, Glasgow, UK G1 1XL*
[b]*Centre for Molecular & Interface Engineering, Department of Mechanical and Chemical Engineering, Heriot-Watt University, Edinburgh, UK EH14 4AS. E-mail: k.j.roberts@hw.ac.uk*
[c]*Infineum UK Limited, Milton Hill, Abingdon, Oxfordshire, UK OX13 6BB*
[d]*CCLRC Daresbury Laboratory, Warrington, UK WA4 4AD*

Received 9th March 1999, Accepted 8th June 1999

Differential scanning calorimetry and variable temperature high-resolution X-ray powder diffraction using synchrotron radiation are used to identify the solid-state phase transitions occurring in real diesel wax systems and correlated with the structural packing of these systems. The waxes are found to undergo three solid-state phase transitions. The first involves a partial transition of some of the *n*-alkane fraction from the stable low temperature orthorhombic structure in which the waxes pack with four molecules per unit cell and space group *Fmmm* to the high temperature rotator phase. The second, previously unidentified, transition reflects this phase separation behaviour within the multi-homologous wax mixtures probably associated with the aggregation of highly ordered lamellae of similar chain lengths which are able to maintain the low temperature orthorhombic phase over a higher temperature range before transforming into the rotator phase. The final transition reflects the transformation of the rotator phase to the molten state. A molecular scale packing model consisting of aggregates of similar *n*-alkane chain lengths and aggregates of differing chain lengths is proposed to account for this phenomenon.

1. Introduction

Normal alkanes form the basic building block unit in most naturally occurring organic linear chain molecular systems; such as, wax fractions from petroleum, biological lipids, soaps, fats and linear polymers. In an attempt to understand the solid-state structure of these natural materials more clearly, studies have been undertaken to investigate the structure of crystalline *n*-alkane single homologues.[1] These studies have revealed that these materials crystallise in the form of thin plates with regular faces in which the chain direction is more or less perpendicular to the lamella surface. In the solid state the *n*-alkanes (C_nH_{2n+2}) in general[11] adopt three structurally distinct groups: triclinic [$12 < n(\text{even}) < 26$], orthorhombic [$n(\text{even}) \geqslant 36$ and $n(\text{odd})$] and monoclinic [$28 < n(\text{even}) \leqslant 36$]. Prior to melting the alkanes are known to exhibit solid–solid phase transitions to crystalline 'rotator' phases[2] in which the chains undergo hindered rotation about the main carbon axis and the molecules adopt a packing motif close to a hexagonal structure.

While these results have offered some insight into understanding the solid state structure of the naturally occurring linear chain molecules, these natural systems tend to be composed of polydispersed aggregates rather than of single homologues. As a result, much research has been undertaken, using a variety of techniques,[3–15] to investigate the ability of *n*-alkanes to form multi-homologous crystalline aggregates. Recent studies of binary mixtures of *n*-alkanes have revealed that in the liquid state all chain lengths are fully miscible, while in the solid phases the miscibility is strongly influenced by the carbon number difference and odd–even carbon number effects.[7,8,14] For example, for binary systems with carbon number differences of greater than five carbon atoms the homologues tend to demix in the solid phase to form lamellae composed of the single homologues. For shorter chain length differences, the studies have shown that despite the chain length mismatches present within the lamellae, the lamella surface is still ordered enough to allow for further nucleation of subsequent layers. Models involving interchain mixing, resulting in conformational disorder along the 001 plane, or chain migration have arisen to account for this process; however, the exact mechanism for crystallisation is still not fully understood.

In a previous paper,[3] we presented our investigations using high-resolution synchrotron X-ray powder diffraction to determine the unit-cell parameters of binary (n-$C_{20}H_{42}$–n-$C_{21}H_{44}$ and n-$C_{20}H_{42}$–n-$C_{22}H_{46}$), tertiary (n-$C_{19}H_{40}$ to n-$C_{21}H_{44}$ and n-$C_{20}H_{42}$ to n-$C_{22}H_{46}$) and quinternary (with *n*-alkanes ranging from n-$C_{18}H_{38}$ to n-$C_{26}H_{54}$) *n*-alkane mixed homologous systems, together with a number of real diesel waxes. In this study we found that all the structures conformed to the orthorhombic structure with four molecules per unit cell and space group *Fmmm* predicted by Luth *et al.*[11] for binary mixtures. Line profile analysis of the powder patterns revealed the existence of incipient end-chain and interchain disorder; a crystal packing model consisting of interchain mixing, end-chain twisting and chain migration was proposed to account for the observed disorder. For the real diesel waxes studied at ambient temperatures two crystalline phases were found to exist. The lower molecular weight waxes crystallised to form a high temperature orthorhombic phase (βo-phase), while the higher molecular weight waxes formed the low temperature phase (β-phase) and in a few of the intermediate molecular weight systems these two phases were found to co-exist.

The work carried out so far has generally been based on the analysis of static systems. Whilst some attempts have been made to study the phase transition phenomenon in petroleum waxes, these have however been limited, providing scant

†*Present address*: Blacksmith (A Division of Champion Blacksmith), Minto Ave., Aberdeen, UK AB1 4JZ.

information on the structural nature of solid–solid and solid–liquid interactions. Up till now there have been no detailed studies which attempt to correlate the phase transformation behaviour of multi-homologous waxes with their composition and structure. Most investigations in this area have been restricted to studies of well-characterised wax systems.[15–17] In this paper we investigate the phase transitions and the disorder characteristics for real diesel waxes using differential scanning calorimetry (applied to 22 real diesel wax systems) and variable temperature high resolution synchrotron X-ray powder diffraction (six diesel wax case studies) techniques. This work is aimed towards defining the kinetics of the phase transformation behaviour of these waxes in order to more fully understand the anomalous rotator phase transition behaviour (β to βo) observed in our previous study[3] and to follow any structural changes as a wax approaches the melt state. The overall aim of this study is to present a more complete model of the wax systems so as to be able to account for the stability of the solid-state structures formed.

2. Experimental

2.1 Sample preparation

The real diesel wax samples were supplied by Exxon Chemical Ltd. The sample numbers refer to their industrial classification scheme and are self-consistent with our previous paper[3] as well as the PhD work of one of us.[24] These samples were re-crystallised from diesel fuels and following solid–liquid separation were not further prepared in any way. The detailed sample preparation information is given in the earlier paper.[3] The composition of all samples was determined by gas chromatographic (GC) analysis on an HP 5890 gas chromatograph. Iso-paraffinic impurities in the *n*-alkane waxes were identified and their relative concentrations determined *via* GC mass spectrometry.

2.2 Differential scanning calorimetry

Differential scanning calorimetric (DSC) measurements, using a Dupont model 9900 instrument, were carried out from low temperatures through and beyond the sample melting point. Low temperature runs were effected using a liquid nitrogen jacket. Runs were carried out under a dynamic nitrogen atmosphere at a heating rate of $5\,^{\circ}C\,min^{-1}$. Sample weights used ranged from 10 to 40 mg. Samples were contained in aluminium pans with an empty pan used as a reference side. The DSC was calibrated using pure indium metal (melting point 156 °C). The areas under the transition points were used in the calculation for the heats of fusion and phase transitions.

2.3 Synchrotron X-ray powder diffraction

Powder diffraction patterns were collected using beamline 2.3[18] at Daresbury synchrotron radiation source which has a two-circle diffractometer providing an incremental angular precision of $\pm 0.0001^{\circ}$ and an overall angle measuring accuracy of 0.004°. The patterns were recorded using $\theta/2\theta$ geometry with 2θ ranging from 2 to 60° in steps of 10 millidegrees. The wavelength (1–2 Å range) and zero-point corrections were refined from the positions of the first five peaks observed for a silicon standard and this resulted in a wavelength accurate to 0.00003 Å and a zero-point accuracy in 2θ of 0.0001°. The diffraction scans for each sample were carried out at different temperatures, on a heating and cooling cycle, maintained using a variable-temperature cell. Fig. 1 provides a representative powder pattern taken from these studies, highlighting the superior angular resolution obtained using the synchrotron radiation source.

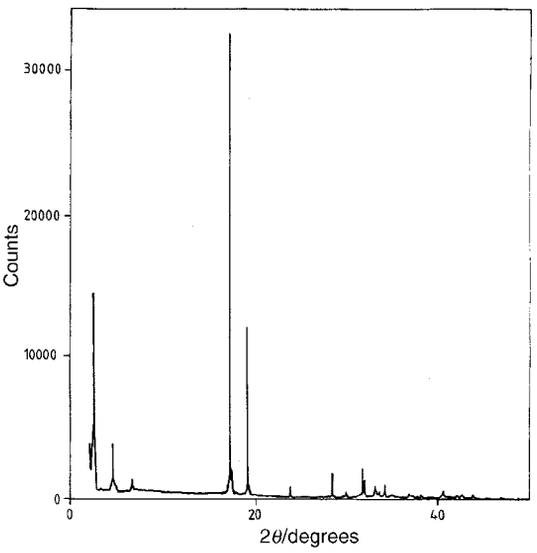

Fig. 1 High resolution X-ray powder diffraction pattern of wax type [80312/86–8] obtained on station 2.3 of Daresbury Synchrotron Radiation Source.

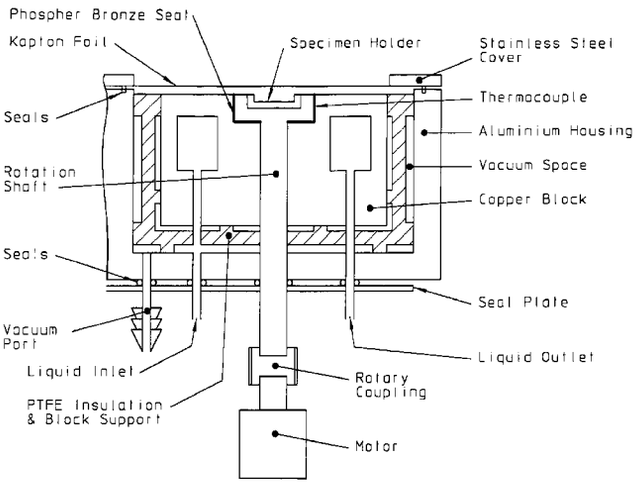

Fig. 2 Schematic of the variable temperature powder diffraction cell used to perform *in-situ* variable temperature high resolution X-ray powder diffraction studies on station 2.3 after ref. 19.

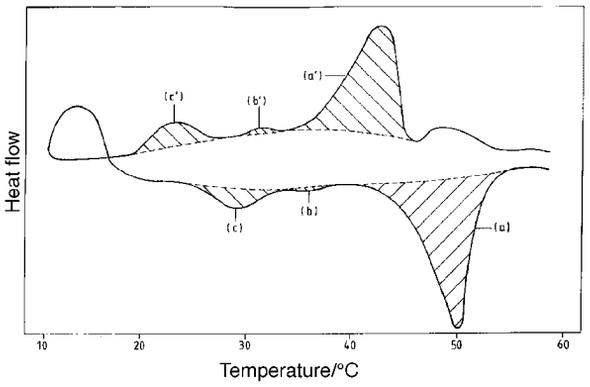

Fig. 3 Differential scanning calorimetry trace of wax type [80442/92+5]. Phase transitions a, b and c represent the melt transition, solid–solid transition and rotator transition states, respectively: a′, b′ and c′ represent the transitions for the reverse cycle.

Table 1 Table of transformation enthalpies for (a) melt, (b) solid–solid and (c) rotator phase changes as a comparison with carbon number average and variance

Wax type	C_n range	Mean C_n	*Vn*	E_a/J g^{-1}	E_b/J g^{-1}	E_c/J g^{-1}
80441/92–18	15–29	20.11	5.50	68.16	0.94	12.88
80074/87–11	15–29	20.73	5.24	171.20	2.85	25.73
80079/87–11	14–29	20.83	5.82	159.20	7.10	24.34
80653/90–14	15–29	21.55	4.32	112.40	2.52	3.07
80708/89–14	15–30	21.96	4.34	147.90	3.70	24.69
80653/90–10	15–29	22.12	4.84	211.60	6.07	14.10
80447/87–10	14–29	22.25	4.82	55.54	1.09	12.40
80308/90–11	17–28	22.54	3.78	139.4	3.75	30.30
80308/90–112	17–29	22.59	3.83	198.40	3.41	24.84
tk186–7	17–29	22.61	3.77	134.2	—	12.59
80312/86–13	15–32	22.82	5.26	94.15	0.47	14.92
80226/89–16a	18–31	23.36	4.67	199.9	2.18	32.76
80291/87–10	18–29	23.57	3.88	207.70	3.31	19.38
80226/89–21	16–30	23.66	5.01	181.1	2.62	16.39
80619/88–8	18–30	23.67	3.89	112.6	1.37	13.30
80312/86–8	15–32	23.67	5.26	177.9	2.94	25.81
80619/88–3	18–30	23.69	3.90	211.4	2.45	17.99
80226/89–16c	15–31	23.92	4.51	190.9	0.91	25.36
80442/92+5	18–32	23.93	4.39	117.9	1.47	19.49
80226/89–11	11–31	24.36	5.38	82.37	—	26.28
89015/91–14	19–32	25.05	4.22	224.6	3.24	33.73
Shell wax	20–37	26.80	7.97	138.9	0.07	30.34

Table 2 Summary table of wax types studied with the different physical properties

Wax	Wax type	C_n range	Mean C_n	Variance	Iso-paraffin content (%)
1	80308/90–11	17–28	22.54	3.78	3.10
2	80226/89–21	16–30	23.66	5.01	2.50
3	80312/86–8	15–32	23.67	5.26	3.35
4	80619/88–8	18–30	23.67	3.89	3.06
5	80442/92–5	18–32	23.93	4.39	3.92
6	89015/91–14	19–32	25.05	4.22	1.89

(a) *In-situ* cell for synchrotron radiation studies. Samples of the waxes for examination on the synchrotron powder diffractometer were held in the specially designed variable-temperature cell shown in Fig. 2 (details given elsewhere[19]) which was mounted on the two-circle diffractometer. Approximately 5 ml of the melt were pipetted in to the sample holder and powder diffraction scans were recorded with a rotating sample in order to average out the effects of preferred orientation. The temperature of the sample cell was controlled by an integral water jacket fed from a Haake F3 recirculating bath (accurate to 0.01°). The rate of heating and cooling effected was controlled by a Haake PG20 temperature programming unit. A series of incremental heating and cooling cycles were carried out in order to follow the nature of the transitional phase changes.

(b) Data reduction and analysis. The data were normalised using the PODSUM program.[20] The peak shapes and resulting peak positions were fitted using a pseudo-Voigt function with the PKFIT program.[20] The unit cell was indexed from the peak positions using the ITO program[21] which is specifically optimised for indexing powder patterns taken from materials having low-symmetry crystal structures. This program provides a figure of merit (F_m) describing the accuracy of the fit to the proposed unit-cell lattice parameters. This is given by eqn (1),

$$F_m = \sum_{l=1}^{n} (Q_{obs} - Q_{calc}) \Big/ \sum_{l=1}^{n} (Q'_{obs} - Q'_{calc}) \qquad (1)$$

where Q is the magnitude of reciprocal lattice vector for each peak as defined by eqn (2),

$$(2\ \sin(\theta)/\lambda)^2 = 1/d^2 = Q \times 10^{-4} \qquad (2)$$

where d is the lattice plane spacing and Q_{obs}' and Q_{calc}' are, respectively, the observed and calculated values for the system. Q_{obs} and Q_{calc} are the same values but for an arbitrary system with the same size reciprocal lattice and n is the number of peaks. A successful indexing is defined by the number of peaks indexed from the first 20 observed and requires the difference between the observed and calculated positions to be $<0.03°$. Following indexing a final refinement of the unit cell parameters were made using the REFCEL program.[20]

In a previous paper[3] we identified the existence of conformational disorders present within the real diesel wax system, arising from the presence of chains with different lengths, which are most evident along the crystallographic *c*-axis direction. In these variable temperature studies, the degree of positional disorder was monitored by determining the isotropic thermal parameter using Wilson's method.[22] In this, the fall-off of the relative diffracted intensity, with respect to

Table 3 Approximate temperature ranges for the solid–solid phase transitions obtained from DSC for the different wax types; (a, a′) melt, (b, b′) solid–solid and (c, c′) rotator phase changes

	Cooling cycle Temperature range/°C			Heating cycle Temperature range/°C		
Wax	a	b	c	a′	b′	c′
1	45.0–40.0	29.0–25.5	19.5–15.0	33.0–38.5	24.0–26.0	9.5–15.0
2	48.5–41.5	35.0–33.0	29.0–25.0	37.0–42.0	29.0–31.0	18.5–24.0
3	58.0–50.0	46.0–44.0	38.5–35.0	39.0–44.0	31.0–33.0	21.5–26.5
4	50.0–46.0	36.0–34.5	29.5–27.0	39.0–44.0	34.5–36.0	21.5–24.5
5	51.0–48.0	36.5–34.5	31.5–27.4	39.0–45.0	30.5–32.0	21.5–25.5
6	51.5–46.5	35.5–34.5	34.0–30.5	47.5–49.0	34.5–35.5	21.5–30.5

Table 4 Unit cell parameters, fitting factor (F.F.), molecular volume (Vm) and Wilson plot disorder (U^2) for the heating–cooling cycle for wax 1 [type 80308/90–11]; all numbers enclosed in ( ) are the standard deviations of the lattice parameters directly above

a/Å	b/Å	c/Å	Temp./°C	F.F.	Vm/Å^3	Phase	$(b/a)^2$	U^2/Å^2
4.995	7.443	62.232	5.04	0.61	2314	β	2.220	6.80
(0.003	0.002	0.032)						
5.004	7.468	62.370	14.07	0.34	2331	β	2.227	7.09
(0.001	0.001	0.018)						
5.028	7.617	62.317	20.26	0.27	2387	βo	2.295	7.85
(0.001	0.001	0.020)						
4.975	7.778	62.336	28.26	0.13	2412	βo	2.444	7.99
(0.001	0.001	0.010						
—	—	62.417	38.15	—	—	βo	—	8.49
—	—	62.443	39.56	—	—	βo	—	9.06
4.994	7.848	62.337	30.03	0.10	2419	βo	2.520	8.16
(0.001	0.001	0.007)						
5.024	7.639	62.450	22.00	1.11	2397	βo	2.312	8.97
(0.001	0.001	0.008)						
5.028	7.612	62.283	20.24	0.13	2384	βo	2.292	7.53
(0.001	0.005	0.058)						
4.996	7.444	62.232	5.04	0.62	2314	β	2.220	7.17
(0.003	0.002	0.032)						

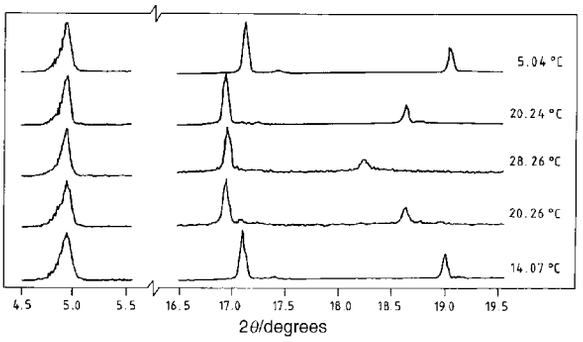

Fig. 4 Stack plot of the variable temperature powder diffraction patterns of wax 1 (type 80308/90–11) showing the phase transition occurring during the heating and cooling cycle: from the low (β) to high (βo) to low (β) temperature orthorhombic states.

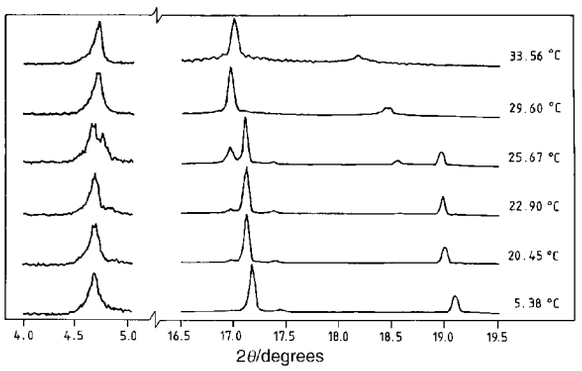

Fig. 5 Stack plot of the variable temperature powder diffraction patterns of wax 2 (type 80226/89–21) showing the phase transitions occurring during the heating cycle: from the low (β) to combined low and high (β/βo) to high (βo) temperature orthorhombic states.

2θ, of a harmonic series of well resolved 001 reflections was examined. An isotropic thermal parameter U was calculated using the relationship given in eqn (3),

$$\ln I_{obs} = \ln C - 4\pi^2 U^2 Q \quad (3)$$

where C is a constant. In this work, the calculated thermal parameter was used as a benchmark to assess whether positional or conformational disorder, brought about by the size differences in chain length mismatches and the number of varying chain lengths, increases or decreases with respect to the solid–solid phase transitions.

The formation of the rotator phase, as the wax samples were heated and cooled, was monitored *via* an examination of the ratio of the two in-plane unit cell parameters *i.e.* $(b/a)^2$. For an *n*-alkane crystallising in an orthorhombic crystal lattice Denicolo *et al.*[23] found $(b/a)^2$ to be nearly constant in the non-rotator crystalline phase but to increase progressively in the rotator phases as the number of carbon atoms in the molecule increased. The upper limit for this ratio can be expected to be 3.0, *i.e.* the theoretical value for the corresponding hexagonal unit cell.

3. Results and discussion

3.1 DSC studies of phase transitions in 'as prepared' wax samples

Twenty-two of the samples taken from the isolated diesel wax systems previously examined at ambient temperatures using X-ray powder diffraction[3] were also analysed by DSC. The aim of this was to characterise the anomalous rotator phases in these materials in an attempt to understand the multiple phase behaviour which was observed in the room temperature studies. Three characteristic phase types were observed from the DSC scans (see representative example in Fig. 3) for most of the wax materials: a, b, and c relating, respectively, to the melt, 'unidentified' and rotator transitions. For each of the 22 diesel crystallised waxes, Table 1 details GC derived compositional parameters together with DSC measured transition enthalpies.

In order to identify the anomalous phase transition shown as an extra peak in between the melting and the rotator phase transition, and to correlate the phase transition with the structural packing, six diesel crystallised wax systems (representing a range of differing compositions) were selected for further analysis using variable temperature high-resolution X-ray powder diffraction.

3.2 Variable temperature X-ray powder diffraction studies of representative wax samples

The six diesel wax systems chosen for analysis using variable temperature synchrotron X-ray powder diffraction, described in our previous paper,[3] were all found to crystallise in an orthorhombic structure in either the β or βo modification. Table 2 summarises their basic physical properties in terms of GC analysis of the range of carbon numbers for the *n*-alkanes in the sample together with the mean and variance of their distribution. Also provided is the measured concentration for the iso-paraffin content in the samples as determined *via* GC mass spectrometry. Table 3 lists the temperature ranges for the solid-state phase transitions observed from the DSC analysis.

Table 5 Unit cell parameters, fitting factor (F.F.), molecular volume (Vm) and Wilson plot disorder (U^2) for the heating/cooling cycle for wax 2 [type 80226/89–21]; all numbers enclosed in ( ) are the standard deviations of the lattice parameters directly above

a/Å	b/Å	c/Å	Temp./°C	F.F.	Vm/Å^3	Phase	$(b/a)^2$	U^2/Å^2
4.986	7.437	66.298	5.38	0.51	2458	β	2.225	7.49
(0.002	0.002	0.030)						
5.000	7.482	66.309	20.00	2.12	2481	β	2.239	7.86
(0.010	0.009	0.126)						
4.998	7.475	66.447	20.45	0.77	2482	β	2.237	7.66
(0.003	0.003	0.045)						
5.023	7.626	63.338	20.45	2.01	2426	βo	2.305	8.50
(0.009	0.008	0.157)						
4.997	7.484	66.381	22.90	0.46	2482	β	2.243	7.90
(0.002	0.002	0.039)						
5.019	7.639	64.222	22.90	1.32	2462	βo	2.317	2.11
(0.006	0.006	0.110)						
5.000	7.488	66.709	25.67	0.86	2498	β	2.243	7.90
(0.004	0.003	0.074)						
5.013	7.656	65.302	25.67	0.21	2506	βo	2.332	4.93
(0.001	0.001	0.018)						
5.001	7.699	65.985	29.60	0.23	2541	βo	2.370	8.53
(0.001	0.001	0.020)						
4.956	7.816	65.985	33.56	0.08	2556	βo	2.487	9.09
(0.000	0.000	0.006)						
—	—	—	39.73	—	—	βo	—	8.08
4.946	7.828	65.666	32.31	0.24	2542	βo	2.505	10.24
(0.001	0.001	0.033)						
5.012	7.642	65.534	25.63	1.49	2510	βo	2.325	8.99
(0.007	0.006	0.208)						
5.005	7.490	—	25.63	1.49	—	β	2.240	—
4.994	7.482	66.192	22.25	0.39	2473	β	2.245	9.94
(0.002	0.002	0.055)						
4.987	7.429	65.584	5.08	0.19	2430	β	2.219	10.79
(0.001	0.001	0.027)						

Table 6 Unit cell parameters, fitting factor (F.F.), molecular volume (Vm) and Wilson plot disorder (U^2) for the heating/cooling cycle for wax 3 [type 80312/86–8]; all numbers enclosed in ( ) are the standard deviations of the lattice parameters directly above

a/Å	b/Å	c/Å	Temp./°C	F.F.	Vm/Å^3	Phase	$(b/a)^2$	U^2/Å^2
4.990	7.452	66.051	10.7	0.76	2456	β	2.230	6.62
(0.004	0.003	0.036)						
5.000	7.482	66.126	22.0	0.54	2474	β	2.239	6.47
(0.003	0.003	0.028)						
5.001	7.498	66.552	25.5	1.51	2496	β	2.248	8.82
(0.008	0.007	0.097)						
5.016	7.644	66.116	25.5	0.51	2535	βo	2.322	—
(0.003	0.002	0.035)						
4.850	7.807	66.745	38.1	2.06	2527	βo	2.591	9.80
(0.008	0.008	0.161)						
4.881	7.726	66.690	34.0	1.09	2515	βo	2.505	8.26
(0.004	0.004	0.086)						
4.992	7.740	66.621	29.5	0.89	2574	βo	2.404	8.82
(0.004	0.004	0.070)						
5.005	7.486	66.598	21.0	1.3	2495	β	2.237	6.20
(0.005	0.005	0.102)						

The unit cell parameters for the six wax systems investigated, as measured as a function of temperature cycling through the various phase transformations that were identified from the DSC examination of the same samples, are summarised in Tables 4–9. For brevity the inter-axial angles ($\alpha=\beta=\gamma=90^\circ$ for the orthorhombic lattice) are omitted from this table.

Wax 1 (type 80308/90–11), below 20 °C is consistent with a low temperature orthorhombic structure (see Table 4), space group $Fmmm$ ($Z=4$). This material melts and re-crystallises as would be typically expected in line with the thermodynamic properties predicted from DSC experiments. The wax crystal expands with increasing temperature, followed by the induced rotator transition indicated from the increasing $(b/a)^2$ value (see also Fig. 4). The cross sectional area of the *n*-alkane chain molecules can be seen to expand dramatically as the lattice is now host to hindered rotation of long chain molecules. Comparing the unit cell parameters for the starting material to those obtained following melt re-crystallisation reveals no change following cycling through the melting point. Likewise the Wilson plot disorder values (U^2) of the initial and final wax structures are approximately the same. This points to the fact that the two structures are isostructural and this is thought to arise for only thermodynamically stable materials that have crystallised to form a stable solid solution. This would suggest that for this particular wax crystal the conditions of crystallisation have produced a very stable eutectic material, whereby the *n*-alkanes are randomly packed throughout the material. This would imply that pre-ordering within the liquid state prior to bulk crystallisation does not exist. The absence of pre-ordering has resulted in a completely random crystallisation mechanism.

No structural anomaly was evident from the temperature studies of wax 1 to account for the unidentified phase transition found in the DSC data taken of the sample. This, together with the stability of the structure of this particular wax, is not consistent with the evidence found for the remaining five waxes.

As shown in Table 5, the unit cell parameters obtained for wax 2 (type 80226/89–21) were subject to thermal expansion as the sample was heated whereby the sample inevitably reached

Table 7 Unit cell parameters, fitting factor (F.F.), molecular volume (Vm) and Wilson plot disorder (U^2) for the heating/cooling cycle for wax 4 [type 80619/88–8]; all numbers enclosed in ( ) are the standard deviations of the lattice parameters directly above

a/Å	b/Å	c/Å	Temp./°C	F.F.	Vm/Å^3	Phase	$(b/a)^2$	U^2/Å^2
4.996	7.460	64.970	10.0	0.55	2421	β	2.230	5.64
(0.003	0.002	0.024)						
5.002	7.491	65.620	22.0	0.85	2459	β	2.243	5.39
(0.004	0.003	0.049)						
5.020	7.639	64.739	22.0	0.50	2483	βo	2.316	4.95
(0.002	0.002	0.028)						
5.006	7.698	65.143	27.0	0.36	2510	βo	2.365	5.68
(0.002	0.002	0.021)						
4.954	7.828	65.148	32.0	0.05	2526	βo	2.497	5.88
(0.001	0.001	0.003)						
5.299	8.732	71.840	36.0	0.23	3324	βo	2.715	11.09
(0.001	0.001	0.021)						
—	—	66.545	35.18	—	—	βo	—	6.47
—	—	66.009	27.00	—	—	βo	—	6.46
—	—	65.993	22.25	—	—	βo	—	5.55
4.990	7.467	65.741	10.36	0.49	2450	β	2.239	4.50
(0.002	0.002	0.028)						

Table 8 Unit cell parameters, fitting factor (F.F.), molecular volume (Vm) and Wilson plot disorder (U^2) for the heating/cooling cycle for wax 5 [type 80442/92+5]; all numbers enclosed in ( ) are the standard deviations of the lattice parameters directly above

a/Å	b/Å	c/Å	Temp./°C	F.F.	Vm/Å^3	Phase	$(b/a)^2$	U^2/Å^2
4.989	7.453	65.844	10.47	0.85	2448	β	2.232	7.66
(0.004	0.004	0.054)						
5.002	7.481	66.015	20.44	0.46	2470	β	2.237	7.65
(0.002	0.002	0.029)						
4.995	7.487	66.111	22.40	0.44	2472	β	2.247	7.79
(0.002	0.002	0.028)						
5.003	7.493	66.247	24.43	0.32	2483	β	2.243	8.07
(0.002	0.001	0.015)						
—	—	60.872	24.43	—	—	βo	—	—
5.008	7.498	65.972	26.43	1.18	2477	βo	2.242	8.74
(0.006	0.005	0.074)						
5.007	7.687	66.075	28.37	0.25	2543	βo	2.357	8.30
(0.001	0.001	0.016)						
5.012	7.729	66.181	30.36	0.74	2564	βo	2.378	8.83
(0.004	0.004	0.047)						
4.949	7.839	66.287	33.33	0.42	2572	βo	2.509	8.47
(0.002	0.002	0.026)						
—	—	66.467	37.42	—	—	βo	—	6.58
4.949	7.838	66.509	33.45	0.27	2580	βo	2.508	7.71
(0.001	0.001	0.025)						
4.998	7.733	66.399	30.94	0.29	2566	βo	2.394	7.35
(0.001	0.001	0.027)						
5.021	7.635	63.692	26.06	1.44	2442	βo	2.312	4.13
(0.007	0.007	0.124)						
5.004	7.493	66.556	26.06	0.15	2496	β	2.242	6.93
(0.001	0.001	0.014)						
5.001	7.488	66.434	23.06	0.65	2488	β	2.242	6.13
(0.003	0.003	0.061)						
4.991	7.452	66.337	10.00	1.10	2467	β	2.229	5.85
(0.005	0.005	0.070)						

the rotator state. On appearance of the rotator transition, two structures can be seen to co-exist simultaneously (see Fig. 5). As the temperature reaches the first rotator transition, the wax segregates into the low and high temperature (β and βo) orthorhombic forms. It is clear, therefore, that only part of the wax system is induced into the rotationally distorted phase, whilst the other region remains in the static crystalline state. Further heating induces the residual low temperature orthorhombic phase into its rotator state. This second transition can now be identified as the second unidentified transition within the DSC plot. This phase behaviour is found to be reversible upon cooling although a certain degree of hysteresis exists.

A possible explanation for this behaviour is that a certain degree of pre-ordering exists among the crystallising *n*-alkanes within the diesel mixture. This effect, observed for binary mixture *n*-alkanes,[14] is produced when clusters of similar chain length *n*-alkanes freeze out of the liquid state resulting in pockets of like-sized molecules clustering within the wax crystallite. Upon heating, once the rotator transition has occurred, the more stable regions of like-sized molecules will preserve their structural integrity, and resist the thermodynamic driving force to adopt the hindered rotational state, whereas the regions that do not possess clustering are induced into the rotator state. The clustered packing states remain in the low temperature orthorhombic state until further heating induces their unique rotator transition point at a higher temperature (observed as an extra phase transition), and only from this point does the wax behave as an equivalent system.

The initial and final re-crystallised wax *c*-axis lattice parameters, for wax 2, vary by 0.714 Å, and the total molecular volume dropped by 28 Å^3. This indicates that the molecules are somehow adopting a tighter, more efficiently packed structure. This would suggest that, as a result of heating the solid wax, the extremely mobile *n*-alkanes have re-arranged to a certain extent in the liquid and solid state. A degree of molecular migration, found for binary mixtures of *n*-alkanes,[7,8,14] has occurred

Table 9 Unit cell parameters, fitting factor (F.F.), molecular volume (Vm) and Wilson plot disorder (U^2) for the heating/cooling cycle for wax 6 [type 89015/91–14]; all numbers enclosed in ( ) are the standard deviations of the lattice parameters directly above

a/Å	b/Å	c/Å	Temp./°C	F.F.	Vm/Å^3	Phase	$(b/a)^2$	U^2/Å^2
4.976	7.425	68.768	−2.00	0.62	2541	β	2.227	3.63
(0.002	0.002	0.022)						
4.984	7.448	68.862	10.00	0.83	2556	β	2.233	4.20
(0.003	0.003	0.030)						
4.990	7.472	68.856	20.00	0.81	2567	β	2.242	4.51
(0.003	0.003	0.029)						
4.995	7.486	68.944	25.00	0.54	2578	β	2.246	3.98
(0.002	0.002	0.019)						
4.998	7.502	69.011	30.00	0.66	2588	β	2.253	4.08
(0.002	0.002	0.032)						
5.000	7.508	69.234	32.00	1.07	2599	β	2.255	4.21
(0.004	0.003	0.052)						
5.000	7.699	68.291	32.00	0.44	2629	βo	2.371	2.22
(0.002	0.001	0.023)						
4.985	7.747	68.909	35.00	0.58	2661	βo	2.415	4.67
(0.002	0.002	0.028)						
—	—	68.694	40.00	—	—	βo	—	4.24
4.968	7.785	68.796	36.00	1.16	2661	βo	2.456	4.69
(0.004	0.004	0.056)						
5.000	7.697	68.592	33.00	1.11	2640	βo	2.370	4.64
(0.004	0.004	0.053)						
4.994	7.511	69.068	33.00	6.91	2591	β	2.262	0.83
(0.026	0.021	0.370)						
5.003	7.680	67.610	30.00	0.44	2598	βo	2.356	2.77
(0.002	0.001	0.032)						
4.997	7.503	68.837	30.00	0.35	2581	β	2.255	4.29
(0.0012	0.001	0.025)						
4.993	7.485	68.681	25.00	0.93	2567	β	2.247	4.85
(0.0032	0.0029	0.0447)						
4.990	7.472	68.605	20.00	0.95	2558	β	2.242	4.19
(0.003	0.003	0.046)						
4.984	7.446	68.468	10.00	0.88	2541	β	2.232	4.19
(0.001	0.003	0.042)						
4.975	7.421	68.379	−2.00	0.81	2525	β	2.225	3.91
(0.003	0.002	0.039)						

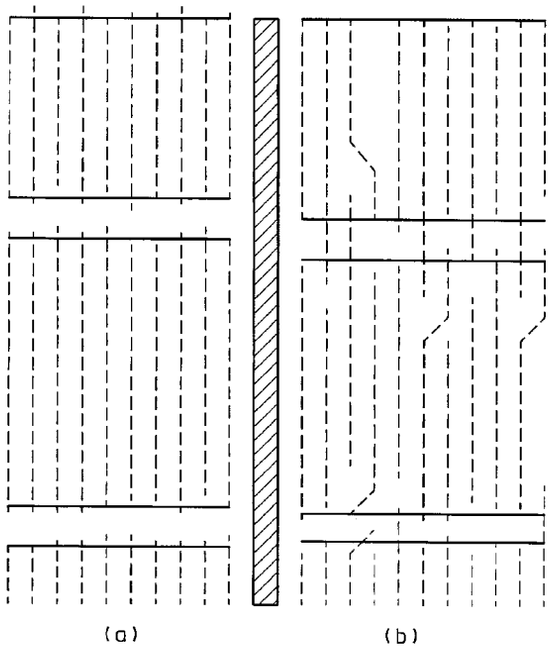

Fig. 6 Possible crystal packing model for the wax systems indicating (a) areas of highly ordered lamellae formed of *n*-alkanes of similar chain lengths in which the interlamellar region is relatively ordered, and (b) lamellae formed from *n*-alkanes of very different chain lengths with a highly disordered interlamellar region resulting from end-chain protrusions of the longer chain lengths. For the future we hope to be able to model this and predict the effect on diffraction patterns.

whereby more lamellae of like-sized chain lengths have been created, resulting in less disordering of adjacent chain packing as the number of voids (due to packing of adjacent molecules of large chain length difference) is reduced. However, as the number of voids within lamellae decreases, this would result in a greater degree of disorder in the inter-lamellar region as the possibility of interchain mixing from adjacent lamellae is reduced.

As with wax 2, waxes 3 (type 80312/86–8), 4 (type 80619/88–8) and 5 (type 80442/92–5) upon heating enter the rotator transitional state with the formation of the high temperature orthorhombic form, while the low temperature orthorhombic form remains relatively stable prevailing over a higher temperature range (see Tables 6–8). The rotator melt transition for the low temperature form is reached with further heating, adopting the classical pseudo-hexagonal packed rotator phase. The manner in which the diffraction peaks split for these waxes is seen to be reversible although a small amount of hysteresis does exist, whereby the resultant re-crystallised structures are found to be different from the initial starting structures.

A slightly different type of behaviour was observed for waxes 3 to 5 as compared to wax 2. The resulting *c*-axis parameters were found to expand indicating an enlarged structure, also observed as an overall increase in the lattice volume, and the Wilson plot disorder dropped suggesting a decrease in the overall disorder within the inter-lamellae regions.

The explanation for this slight difference in behaviour is not, at first glance, obvious. However, a possible explanation could be found in the percentage of residual iso-paraffin content observed in each of the wax systems: the percentages found in waxes 3 to 5 are noticeably higher than that found in wax 2. Possible interpretations for this crystallisation mechanism could be connected to the wax approaching the melt phase whereby residual trapped solvent could sweat out of the lamellae. Although the solvent is not thought to disrupt the

structural nature of the crystallising wax, it could be thought to disrupt the inter-lamellae region. This could potentially force the lamellae to adopt wider spacing, resulting in an extended *c*-axis length thus minimising the conformational disorder arising from end-chain bending and folding within this region.

Wax 6 (type 89015/91–14) behaves in a similar manner to wax 2. From the cell parameters in Table 9 it is evident that the two phase system persists above the first rotator phase transition, as the temperature is increased further the entire system adopts the pseudo-hexagonal packing structure. When comparing the initial and final wax crystalline material (both held at the same temperature), once again the reformed melt crystalline wax is found to have a different structure. The lattice adopts a smaller molecular volume resulting in the subsequent increase in the Wilson plot parameter. The molecular volume difference can be accounted for by the different *c*-axis parameter varying by 0.411 Å. This has been shown to result in a tighter packed structure, and indicates that the lamella region will be disrupted as a consequence of the longer *n*-alkanes protruding into the lamellae.

4. Conclusions

Six waxes have now been studied using variable temperature X-ray powder diffraction, and their phase transformation behaviour identified from DSC measurement has now been correlated to structural transformations to and from the β and βo phases. In general, these wax samples were found to exhibit three phase changes, two of which have been well characterised. The additional solid-state phase change was found to be consistent with the result of molecular pre-ordering within the wax as a result of clustering of similar chain length *n*-alkanes. A possible model for the wax crystallites composed of highly ordered areas with similar chain length lamellae and clusters with large chain length differences is given in Fig. 6.

The low temperature orthorhombic form (β) was seen to possess higher disorder in the lamella region than its rotator state counter-part (as the crystalline aggregates composed of *n*-alkanes of very different chain lengths [Fig. 6(b)] reach the rotator state the mobile alkanes are able to fully extend their structure thus minimising the need for end chain bending or folding). When progressing into the rotator region, the appearance of a high temperature orthorhombic state (β_0) emerges whereby there still exists a residual β-state. This residual β-state exists with a lower disorder value U^2 (compared to that of the original) indicating, at least, a better packed lamella region. This could be the result of crystalline aggregates of similar chain lengths packing in a more energetically favourable and ordered manner, maintaining their structural integrity. These packing regions of greater stability can exist with temperatures much higher than the initial rotator temperature, indicative of the higher packing stability known to be maintained.

After the successful re-crystallisation of the wax was achieved, the resultant material was found to possess a different lattice parameter. This could be due to a combined molecular migration process within the solid and liquid states in which further aggregates of lamellae with similar chain lengths are formed (comparable with the demixing process found for binary alkanes[14]). This could either reflect the complex structural nature of these multi-homologous phases or perhaps the action of impurity species. Either of these could potentially inhibit the crystallisation process thus not permitting the wax crystal lattice to adopt its lowest energy state. Thus one could envisage a process whereby the growth from the melt phase would differ significantly enough from the sample's initial solution crystallisation from diesel fuel such that the *n*-alkanes would be able to migrate and pack with different preferred molecular packing motifs. One way of verifying this theory would be to repeatedly heat and cool the wax from the melt to see if a more stable equilibrium structure was formed and/or to observe the same process during an associated solution phase re-crystallisation from diesel fuels.

While chain migration associated with the formation of highly ordered lamellae with *n*-alkanes of similar chain lengths is to a degree occurring during crystallisation, DSC data suggest that the concentration of these is quite small. The latter can be seen by the fact that the second rotator state transition is small compared to the first transformation. This would suggest that the overall wax forms stable crystallites composed of varying chain lengths. A model for this packing structure has been proposed in a previous paper.[3]

Acknowledgements

Research towards improving our understanding of the structural aspects of wax crystallisation has been supported for a number of years through research grants from both the EPSRC and Exxon Chemical Ltd. We gratefully acknowledge Exxon Chemical Ltd. for the financial support of a PhD studentship (SRC),[24] EPSRC for providing beam time on the Daresbury SRS and for their financial support of a studentship (GPH). We are also grateful to David Watson's group in the Pharmacy Department at Strathclyde who carried out the GC Mass Spectrometry analysis of the iso-paraffin content in the wax samples for us.

References

1 S. R. Craig, G. P. Hastie, K. J. Roberts and J. N. Sherwood, *J. Mater. Chem.*, 1994, **4**, 997; S. R. Craig, G. P. Hastie and K. J. Roberts, *J. Mater. Sci. Lett.*, 1996, **15**, 1193.
2 H. E. King Jr., E. B. Sirota, H. Shao and D. M. Singer, *J. Phys. D: Appl. Phys.*, 1993, **26**, B133.
3 S. R. Craig, G. P. Hastie, K. J. Roberts, A. R. Gerson, J. N. Sherwood and R. D. Tack, *J. Mater. Chem.*, 1998, **8**, 859.
4 I. Denicolo, A. F. Craievich and J. Doucet, *J. Chem. Phys.*, 1984, **12**, 80.
5 M. Dirand, Z. Achour, B. Jouti, A. Sabour and J. C. Gachon, *Mol. Cryst. Liq. Cryst.*, 1996, **A275**, 293.
6 D. L. Dorset and B. K. Annis, *Macromolecules*, 1996, **29**, 2969.
7 D. L. Dorset and R. G. Snyder, *J. Phys. Chem.*, 1996, **100**, 9848.
8 D. L. Dorset and R. G. Snyder, *Macromolecules*, 1995, **21**, 144.
9 B. Flaherty, *J. Appl. Chem. Biotechnol.*, 1971, **21**, 144.
10 G. P. Hastie and K. J. Roberts, *J. Mater. Sci.*, 1994, **29**, 1915.
11 H. Luth, S. C. Nyburg, P. M. Robinson and H. G. Scott, *Mol. Cryst. Liq. Cryst.*, 1972, **27**, 337.
12 M. Maroncelli, H. L. Strauss and R. G. Snyder, *J. Phys. Chem.*, 1985, **89**, 5260.
13 G. Ungar and A. Keller, *Colloid Polym. Sci.*, 1979, **257**, 90.
14 X. Z. Wu, B. M. Ocko, H. Tang, E. B. Sirota, S. K. Sinha and M. Deutsch, *Phys. Rev. Lett.*, 1995, **75**, 1332.
15 G. Zerbi, R. Piazza and K. Holland-Moritz, *Polymer*, 1982, **23**, 1921.
16 J. Handoo, S. P. Srivastava, K. M. Agrawal and G. C. Joshi, *Fuel*, 1989, **68**, 1346.
17 S. P. Srivastava, R. S. Tandon, D. C. Pandey, D. C. Maadhwal and S. K. Goyal, *Fuel*, 1993, **72**, 1345.
18 R. J. Cernik, P. K. Murray, P. Pattison and A. N. Fitch, *J. Appl. Crystallogr.*, 1990, **23**, 292.
19 S. R. Craig, K. J. Roberts, J. N. Sherwood, K. Sato, M. Iwahashi and R. J. Cernik, *J. Cryst. Growth*, 1993, **128**, 1263; R. J. Cernik, S. R. Craig, K. J. Roberts and J. N. Sherwood, *J. Appl. Crystallogr.*, 1995, **28**, 651.
20 Powder Diffraction Program Library, CLRC Daresbury Laboratory.
21 J. W. Visser, *J. Appl. Crystallogr.*, 1969, **2**, 89.
22 G. H. Stout and L. H. Jensen, X-ray Structure Determination, Wiley-Interscience, New York, 2nd edn., 1989.
23 J. Doucet, I. Denicolo, A. Craievich and A. Collet, *J. Chem. Phys.*, 1981, **75**, 5125.
24 S. Craig, Synchrotron Radiation Studies of the Structure of *n*-Alkanes and Homologous Mixtures, PhD Thesis, University of Strathclyde, 1995.

Paper 9/01827A